BGSG

Volume 58

Research Paper

Correspondence to:
Maria Kouli
mkouli@hmu.gr

DOI number:
http://dx.doi.org/10.12681/bgsg.27058

Keywords:
Thessaly earthquake; Land Surface Temperature; RETIRA; thermal anomalies

Citation:
Kouli, M., Peleli,S., Saltas, V., Makris, J.P. and Valianatos, F. (2021), Robust Satellite Techniques for Mapping Thermal Anomalies Possibly Related to Seismic Activity of March 2021, Thessaly Earthquakes. Bulletin Geological Society Greece, 58, 105-130.

Publication History:
Received: 18/05/2021
Accepted: 05/08/2021
Accepted article online: 07/08/2021

The Editor wishes to thank two anonymous reviewers for their work with the scientific reviewing of the manuscript and Ms Emmanouela Konstantakopoulou for editorial assistance.

ROBUST SATELLITE TECHNIQUES FOR MAPPING THERMAL ANOMALIES POSSIBLY RELATED TO SEISMIC ACTIVITY OF MARCH 2021, THESSALY EARTHQUAKES

Maria Kouli [1,2*], Sofia Peleli [1,2], Vassilis Saltas [1,2], John P. Makris [1,2], Filippos Vallianatos [1,3]

[1] Institute of Physics of the Earth's Interior & Geohazards, UNESCO Chair on Solid Earth Physics and Geohazards Risk Reduction, Hellenic Mediterranean University Research Center, Romanou 3, 73133 Chania, Crete, Greece; saltas@hmu.gr, jpmakris@hmu.gr, sofia.peleli@gmail.com,fvallian@hmu.gr

[2] Hellenic Mediterranean University, Faculty of Electronic Engineering, Romanou 3, Chania, Crete, Greece

[3] National and Kapodistrian University of Athens, Faculty of Geology and Geoenvironment, Department of Geophysics and Geothermics, Athens, 15784 Panepistimiopolis fvallian@geol.uoa.gr

*Correspondence: mkouli@hmu.gr; Tel.: +302821023016

Abstract

In recent years, there is a growing interest concerning the development of a multi-parametric system for earthquakes' short term forecast identifying those parameters whose anomalous variations can be associated to the complex process of such events. In this context, the Robust Satellite Technique (RST) has been adopted herein with the aim to detect and map thermal anomalies probably related with the strong earthquake of M6.3 occurred near the city of Larissa, Thessaly on March 3rd 2021 10:16:07 UTC. For this purpose, 10 years (2012-2021) of daily Night-time Land Surface Temperature (LST) remotely sensed data from Moderate Resolution Imaging Spectroradiometer (MODIS), were analyzed. Pixels characterized by statistically significant LST variations on a daily scale were interpreted as an indicator of variations in seismic activity. Quite intense (Signal/Noise ratio > 2.5) and rare, spatially extensive and time persistent, TIR signal transients were identified, appearing twenty five days before the Thessaly main shock (pre-seismic anomalies: February 6th, February 11th March 1st), the day of the main earthquake (co-seismic anomaly) and after the main shock (post-seismic anomalies: March 4th, 10th and 17th). The final dataset of thermal anomalies

was combined with geological and structural data of the area of interest, such as active faults, composite seismogenic sources, earthquake epicenter and topography in order to perform preliminary spatial analysis.

Keywords: *Thessaly earthquake; Land Surface Temperature; RETIRA; thermal anomalies.*

Περίληψη

Τα τελευταία χρόνια, υπάρχει ένα αυξανόμενο ενδιαφέρον σχετικά με την ανάπτυξη ενός πολυπαραμετρικού συστήματος βραχυπρόθεσμων προβλέψεων σεισμικών γεγονότων συσχετίζοντας τα τελευταία με ανώμαλες μεταβολές παραμέτρων όπως είναι η θερμοκρασία. Σε αυτό το πλαίσιο, η Εύρωστη Δορυφορική Τεχνική (Robust Satellite Technique-RST) έχει υιοθετηθεί εδώ με σκοπό την ανίχνευση και χαρτογράφηση πιθανών θερμικών ανωμαλιών που σχετίζονται χωροχρονικά με τον ισχυρό σεισμό μεγέθους Μ6.3 που συνέβη 20 km ΒΔ της πόλης της Λάρισας, στις 3 Μαρτίου 2021 και ώρα 10:16:07 UTC. Το σύνολο των δεδομένων που αναλύθηκε καλύπτει μια χρονική περίοδο δέκα ετών (2012-2021) νυχτερινών καταγραφών LST (Land Surface Temperature) του φασματοραδιόμετρου MODIS (Moderate Resolution Imaging Spectroradiometer). Τα εικονοστοιχεία που χαρακτηρίζονται από στατιστικά σημαντικές μεταβολές LST σε καθημερινή κλίμακα ερμηνεύθηκαν ως πιθανοί δείκτες διακυμάνσεων της σεισμικής δραστηριότητας. Αρκετά έντονες θερμικές ανωμαλίες με λόγο σήματος προς θόρυβο μεγαλύτερο του 2.5 και σπάνιες, χωρικά εκτεταμένες και χρονικά ανθεκτικές θερμικές μεταβολές εμφανίζονται 25 ημέρες πριν από το κύριο σεισμό της Θεσσαλίας και συγκεκριμένα την 6η Φεβρουαρίου, 11η Φεβρουαρίου και 1η Μαρτίου, την ημέρα του κύριου σεισμού καθώς και έως και 14 ημέρες μετά τον κύριο σεισμό (μετασεισμικές ανωμαλίες την 4η, 10η και 17η Μαρτίου). Το σύνολο των θερμικών ανωμαλιών συνδυάστηκε με άλλα δεδομένα, όπως η γεωλογία, η τοπογραφία, τα ενεργά ρήγματα και οι σύνθετες σεισμικές πηγές της περιοχής ενδιαφέροντος προκειμένου να πραγματοποιηθεί μια προκαταρκτική χωρική ανάλυση.

Λέξεις-κλειδιά: *Σεισμός Θεσσαλίας; Θερμοκρασία Εδάφους; Εύρωστη Δορυφορική Τεχνική (Robust Satellite Technique-RST); δείκτης RETIRA; θερμικές ανωμαλίες.*

1. INTRODUCTION

Looking toward the assessment of a multi-parametric system for tectonic deformations' short term (from days to weeks) forecast, a preliminary step is to identify those

parameters (chemical, physical, biological, etc.) whose anomalous variations can be, to some extent, associated to the complex process of preparation of such a tectonic event (Genzano et. al., 2020). A candidate parameter for integration in such a multiparametric system should: i) be selected on the basis of experimental observations, ii) be measurable with sufficient space-time continuity, iii) exhibit space-time transients (potentially related to earthquakes) identifiable through clear, scientifically founded and repeatable data analysis techniques and iv) exhibits a non-occasional relation between space-time transients and earthquake characteristics (e.g. time, position, magnitude) (Genzano et al., 2020).

Among the different parameters, the fluctuations of Earth's thermally emitted radiation, as measured by sensors on board of satellite systems operating in the Thermal Infra-Red (TIR) spectral range has been proposed since long time as a potential precursor. Satellite remote sensing enables the estimation of Land Surface Temperature (LST) over wide areas and especially in sites with different land surface characteristics such as vegetation cover, topography, lithology, tectonic structure and geomorphometry, with a variable spatio-temporal resolution depending on the selected satellite/sensor system (Li et al., 2013). Satellite sensors, as MODIS (Moderate Resolution Imaging Spectroradiometer), having channels in the infrared region of the electromagnetic spectrum, enable the monitoring of the Earth’s thermal field at a moderate spatial resolution (Lillesand et al., 1987; Anderson et al., 2012; Vollmer and Möllmann, 2017). As a result, LST can greatly contribute to the understanding of land surface processes in various scales (from local to global) (Brunsell and Gillies, 2003; Anderson and Kustas, 2008; Kustas and Anderson, 2009; Karnieli et al., 2010; Ganas et al., 2010; Keramitsoglou et al., 2011; Zhang et al., 2014; Christman et al., 2016; Scambos et al., 2018; Eleftheriou et al., 2016b; Aguilar-Lome et al., 2019; Athanasiadou et al.,2020; Peleli et al., 2021).

Since 2001, a general approach called Robust Satellite Techniques (RST) (Tramutoli et al., 2001; 2005; 2007) has been used to discriminate anomalous thermal signals, possibly associated to tectonic activity from normal fluctuations of Earth's thermal emission related to other causes. The RST considers each anomaly in the space-time domain as a deviation from a normal state that can be defined by processing multi-year time series of homogeneous (e.g., same month, same spectral channel/s; same overpass times) cloud-free satellite records. As shown in several papers (e.g., Tramutoli et al., 2001, 2005, 2009, 2015b, 2018b; Filizzola et al., 2004; Eleftheriou et al., 2016a; Genzano et., 2020; Peleli et al., 2021), differently from other approaches, the RST methodology is able to isolate residual TIR variations which are potentially related to

seismic events. During the last 20 years, the RST technique has been applied to four different continents and many geo-tectonic contexts, in several earthquakes with magnitudes ranging from 4.0 to 7.9, using both polar (NOAA-AVHRR, EOS-MODIS) and geostationary (MFG-MVIRI, MSG-SEVIRI, GOES-IMAGER, MTSAT-IMAGER) satellite data, revealing correlations between TIR anomalies and tectonic deformation, in a time window ranging from 30 days before to 15 days after a seismic event (Genzano et al., 2020 and references therein). Nevertheless, remote sensing techniques for several reasons cannot perform identically well everywhere, every time (e.g. due to the presence of clouds). For this reason, sometimes the satellite-based research approaches have been the object of criticism (e.g. Pavlidou et al., 2019). From the other hand, a quite solid study performed by a group with a multi-decade experience in this specific field suggests that TIR variations have a non-casual relation with earthquakes' occurrence. For instance, Filizzola et al. (2004) reported TIR anomalies related to the M~5.9 Athens earthquake of 7 September 1999. Similarly, Tramutoli et al. (2005) applied the RST methodology for the M7.8 Izmit earthquake on 17 August 1999. Pergola et al. (2010) detected thermal anomalies a few days before the Abruzzo (Italy) earthquake occurred on 6 April 2009 (M5.8). Moreover, the long-term analysis (10 years of continuous data over Greece, with a false positive rate of 7%) performed by Eleftheriou et al. (2016a) revealed the generic correlation among earthquakes and RST calculated thermal anomalies.

In the current study, RST has been adopted with the aim to detect and map thermal anomalies probably related with one of the most significant earthquake sequences recorded in northern Thessaly, near the city of Larissa during March of 2021 (for details about Thessaly sequence and its impact please refer to Ganas et al., 2021 and Mavroulis et al., 2021). The sequence included a M6.3 main event on March 3rd 2021, 10:16:07 UTC which was followed by a M6.0 event after 32 hours and a M5.6 event on March 12 and thousands of smaller aftershocks. For this purpose, 10 years (2012-2021) of daily Night-time Land Surface Temperature (LST) remotely sensed data from Moderate Resolution Imaging Spectroradiometer (MODIS), were analyzed.

2. GEOTECTONIC SETTING

The Province of Thessaly comprises the most extended plain in the Greek peninsula. Its terrain is divided into the Plain of Trikala-Karditsa to the west and the Plain of Larisa to the east. The Pinios River drains the entire Basin of Thessaly (Fig.1a). On March

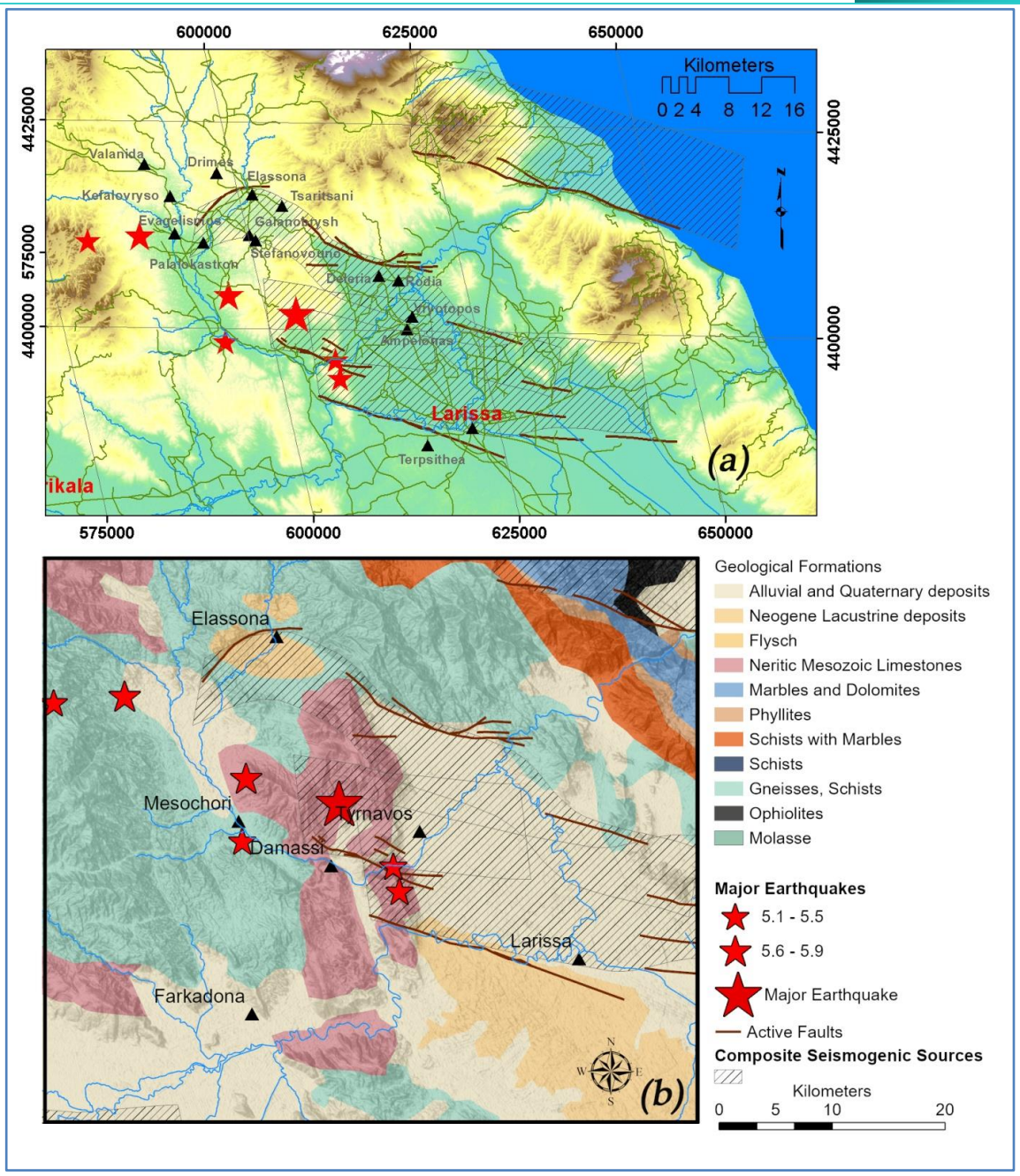

Fig. 1: (a) The SRTM elevation model (Shuttle Radar Topography Mission Void Filled (DOI: /10.5066/F7F76B1X downloaded from https://earthexplorer.usgs.gov/) and (b) the geological map of the study area, with overlay of the major earthquakes obtained from European Mediterranean Seismological Centre, the major active faults (adopted from Ganas et al., 2013) and the seismogenic sources (adopted from Caputo and Pavlides, 2013) located in the area.

3rd 2021 10:16:07 UTC, a strong earthquake (M 6.3) occurred 20 km NW of the city of Larissa. Another strong earthquake occurred on March 4th 18:38:19 UTC (M 5.8) in the same area. Consequently, many damages were caused by the seismic activity affecting thousands of people (Fig.1a). The most serious damages occurred near Damassi and other villages located along the banks of Titarissios river. The broader area exhibits geological complexity and intense tectonic deformation (Athanassiou,

2002) (Fig. 1b). The plain is covered by a thick alluvium layer which represents a significant mantle of beds in the rivers and the streams (Athanassiou, 2002; Vassilopoulou et al., 2013). The Quaternary deposits can be classified to: alluvial sediments that cover the plain of Larissa, fluvial terraces (Penios river) and lacustrine deposits. Mesozoic carbonates (karstic limestones and marbles) and Paleozoic Metamorphic formations (gneiss, schists and amphibolites) are underlain the Neogene deposits. The simplified geology of the area is given in Fig. 1, after Athanassiou, 2002. After the Alpine orogenesis, Eastern Thessaly, was affected by a NE–SW extensional regime. As a result, NW–SE elongated horsts and grabens bounded by large normal faults were formed. This tectonic regime is responsible for the NW–SE trending Larissa Basin that dominates the morphology of the region (Caputo et al., 1994). From Middle-Late Pleistocene until now, Thessaly is affected by a N–S lithospheric extension creating a new system of normal faults mainly trending E–W to ESE–WNW (Caputo, 1990, Caputo and Pavlides, 1993). The major consequence of the structural rearrangement was the creation of the Tyrnavos Basin within the Larissa Plain (Caputo et al., 1994). The Tyrnavos Basin has a general E(SE)–W(NW) orientation and it is bordered by two antithetic sets of normal faults, both showing a partial overlapping right-stepping geometry (Caputo, 1995).

3. MATERIALS AND METHODS

The RST (Robust Satellite Techniques; Tramutoli et al., 2005; 2007) technique is a known multi-temporal procedure of satellite data analysis. Its main advantage compared to other methods is the “natural noise” reduction. The source of this “natural noise” can be the water vapor content of the atmosphere or several spatio-temporal changes in land cover, topography and weather conditions. This methodological approach assumes that each spatio-temporal anomaly constitutes a deviation from normality. This deviation/anomaly can be computed by analyzing multiple cloud-free satellite images that meet the same homogeneous characteristics (i.e., same spatial location, same spectral channels, same overpass hours and same day / month for each year) to be comparable to each other. The RETIRA-index, used in this work, is defined as:

$$\otimes_{\Delta T}(r,t') = \frac{\Delta T(r,t') - \mu_{\Delta T}(r)}{\sigma_{\Delta T}(r)} \quad (1)$$

where:

$r = (x,y)$ defines the exact location of each pixel (x,y) on the satellite image,

t' refers to the acquisition time of the satellite image, with $t' \in \tau$, where τ characterizes the homogenous domain of satellite image acquired in the same hour of the day and the same month of the year.

(i) $\Delta T(r,t')$ represents the difference (T(r,t′) -T(t')) of the observed TIR signal value T(x,y,t) with the spatial average T(t) of all the pixels of the satellite image. T(x,y,t) is measured for each pixel of the satellite image (r), while T(t) is calculated in place on the satellite image, without considering the cloudy pixels, all representing the same class of the study area (land or sea) according to where the r is located,

(ii) $\mu_{\Delta T}(r)$ represents the time average and $\sigma_{\Delta T}(r)$ the standard deviation of $\Delta T(r,t')$ measured at site r, computed only on cloud-free pixels from satellite images of the homogenous datasets ($t' \in \tau$).

The RETIRA index provides an estimation of the local (spatial-temporal) excess of the current $\Delta T(r,t')$ signal with its historical computed mean value, weighted by its variability $\sigma_V(x,y)$ at the given location. The latter includes all the possible noise sources, including also the ones that do not have any relationship to the monitored event. The use of $\Delta T(r,t)$ instead of $T(r,t)$ reduces the possible contributions due to daily or yearly meteorological variations (e.g., occasional warming) and/or season time-drifts. The signal (S) is evaluated by comparison with the standard deviation, $\sigma_{\Delta T}$(r). In this way, the signal to noise ratio *(S/N)* can be used to evaluate the intensity of anomalous TIR transients. Tramutoli et al., (2001) showed that the RETIRA index emphasizes low-level thermal anomalies regardless of sources of natural/observational noise.

In many cases, the measurements of TIR anomalies are affected by unexpected natural and/or observational changes such as climatological (e.g., extremely warm days), wildfires, cloud coverage or inaccurate image navigation/co-location. Based on previous literature, (e.g., Filizzola et al., 2004; Tramutoli et al., 2005; Eleftheriou et al., 2016a), one can conclude that RETIRA index (which is based on time-averaged quantities), is sensitive to the abrupt occurrence of signal outliers due to these natural (Aliano et al., 2008a) or observational (see Filizzola et al., 2004; Aliano et al., 2008b) phenomena. However, the specific spatiotemporal characteristics of these signal

variations (small duration, often known date of occurrence and typical spatial distribution) help RETIRA index to define, isolate and highlight the presence of spatiotemporally persistent thermal anomalies even in very low intensity (Tramutoli et al. 2005) and therefore eliminate false alarms.

In this study the MODIS Land Surface Temperature and Emissivity Daily L3 Global 1km (MOD11_A1) product (https://modis.gsfc.nasa.gov/)(i.e., the version 006 (V5)) available from February 24, 2000 was used for the RETIRA index computation. The daily level 3 LST product at 1km spatial resolution is a tile of daily LST product gridded in the Sinusoidal projection. A tile contains 1200 x 1200 grids in 1200 rows and 1200 columns. The exact grid size at 1km spatial resolution is 0.928km by 0.928km (Wan, 2013). This product's spatial resolution guarantees an accuracy of 1 K under cloud-free conditions (e.g., Wan and Dozier, 1996; Wan, 2013). The retrieved MODIS Land Surface Temperature has only non-cloudy pixels due to the use of the MODIS cloud mask product (MOD35_L2 from Terra MODIS or MYD35_L2 from Aqua MODIS) (Wan, 2013). The Scientific Data Sets (SDSs) in the MOD11A1 product are shown in Table 1. The overpass times provided by MODIS LST product are in local solar time, which is defined as the MODIS observation time in coordinated universal time (UTC) plus longitude in degrees divided by 15 (Williamson et al., 2013). MODIS overpass times are converted from local solar time to local standard time or UTC. Night-time LST images (with approximately 00:00 local time of land surface observation in Thessaly) were preferably used because they are affected by soil–air temperature differences to a smaller extent than those acquired a different hour of the day. Moreover, night-time thermal images are less sensitive to local variations of solar illumination and shadows which could be a significant source of land surface temperature variability.

10 years of satellite records (every day of February and March from 2012 to 2021) were incorporated to the RETIRA index computation. The use of long time series satellite data (usually more than 6 years of observations) is absolutely necessary in order to create the thermal background of the region of interest. In detail, during the pre-processing phase, we isolated the "Night-time and Surface Temperature" layer dataset for the ten years' time period and all the images were spatially clipped over the broader earthquake affected area. In this way, 283 images were obtained for the month of February and 310 images for the month of March. Each image contains 5921 non cloudy pixels. The existence of clouds in the images is given as no data value and consequently the number of available pixels reduces as the cloud coverage increases. The images after being spatially subset to the region of interest were checked one by one for the percentage of cloud cover in the specific area as it has been proved that in cases where

the cloudy fraction of the scene exceeds the 80% of the land portion, the remaining values of image constitute the considered signal not representing the real conditions at that given time (Eleftheriou et al., 2016a). Consequently, all the images with a cloud fraction more than 80% were excluded from the final reference field computation. A total of 343 images with a cloud cover of less than 80% were used to calculate the monthly reference fields $\mu_{\Delta T}(x,y)$ and $\sigma_{\Delta T}(x,y)$; 173 images for February and 170 images for March (Figs. 2 and 3 respectively). Subsequently the RETIRA index was calculated for 34 images. Of these, 16 images belong to February while 18 belong to March 2021. The remaining 25 images for the two months of 2021 had a cloud cover of over 80% and as a result were excluded from the procedure. The next step was the on-screen examination of the 34 calculated indices in order to check for the presence of imprinted thermal anomalies. RETIRA is assumed to be a Gaussian standardized variable and the choice of its relative threshold value quantitatively qualifies how much rare (and significant) are the identified anomalies. Anomalous pixels (i.e., pixels of thermal anomaly) were considered those having values of the RETIRA index higher than 2.5. The daily analysis revealed that 9 over the 34 images included anomalous pixels with RETIRA values higher than 2.5.

As already mentioned, the main advantage of RETIRA method over other methods is the reduction of "natural noise". The last one may be due to changes in vegetation, topography and weather conditions. Since these noise sources are eliminated, the extracted thermal anomalies may be associated with intense and rare phenomena such as earthquakes, wildfires and extremely warm days. The time period (February and March) in which we applied this technique helps us to reject the last two phenomena (wildfires and extremely warm days). RETIRA anomalies may be also induced by cloud-coverage and inaccurate image navigation/co-location. Therefore, an assessment of achieved results was performed in order to discriminate true from false thermal anomalies. As a result, 2 out of the 9 images with RETIRA values higher than 2.5 were characterized as false thermal anomalies due to clouds existence. These false thermal anomalies are artifacts characterized from high RETIRA values located along the boundaries of cloudy pixels (violet areas) with the land pixels (Fig. 4). No thermal anomaly image with inaccurate image navigation/co-location was found.

Table 1. The Scientific Data Sets (SDSs) in the MOD11A1 product. (https://icess.eri.ucsb.edu/modis/LstUsrGuide/usrguide.html)

SDS Name	Long Name	Number Type	Unit	Valid Range	Fill Value	Scale factor	Offset
LST_Day_1km	Daily daytime 1km grid	uint16	K	7500-65535	0	0.02	0.0
QC_Day	Quality control for daytime LST and emissivity	uint8	none	0-255	0	NA	NA
Day_view_time	(local solar) Time of daytime Land-surface Temperature observation	uint8	hrs	0-240	0	0.1	0
Day_view_angle	View zenith angle of daytime Land-surface Temperature	uint8	deg	0-130	255	1.0	-65.0
LST_Night_1km	Daily nighttime 1km grid Land-surface Temperature	uint16	K	7500-65535	0	0.02	0.0
QC_Night	Quality control for nighttime LST and emissivity	uint8	none	0-255	0	NA	NA
Night_view_time	(local solar) Time of nighttime Land-surface Temperature observation	uint8	hrs	0-240	0	0.1	0
Night_view_angle	View zenith angle of nighttime Land-surface Temperature	uint8	deg	0-130	255	1.0	-65.0
Emis_31	Band 31 emissivity	uint8	none	1-255	0	0.002	0.49
Emis_32	Band 32 emissivity	uint8	none	1-255	0	0.002	0.49
Clear_day_cov	day clear-sky coverage	uint16	none	0-65535	0	0.0005	0.
Clear_night_cov	night clear-sky coverage	uint16	none	0-65535	0	0.0005	0.

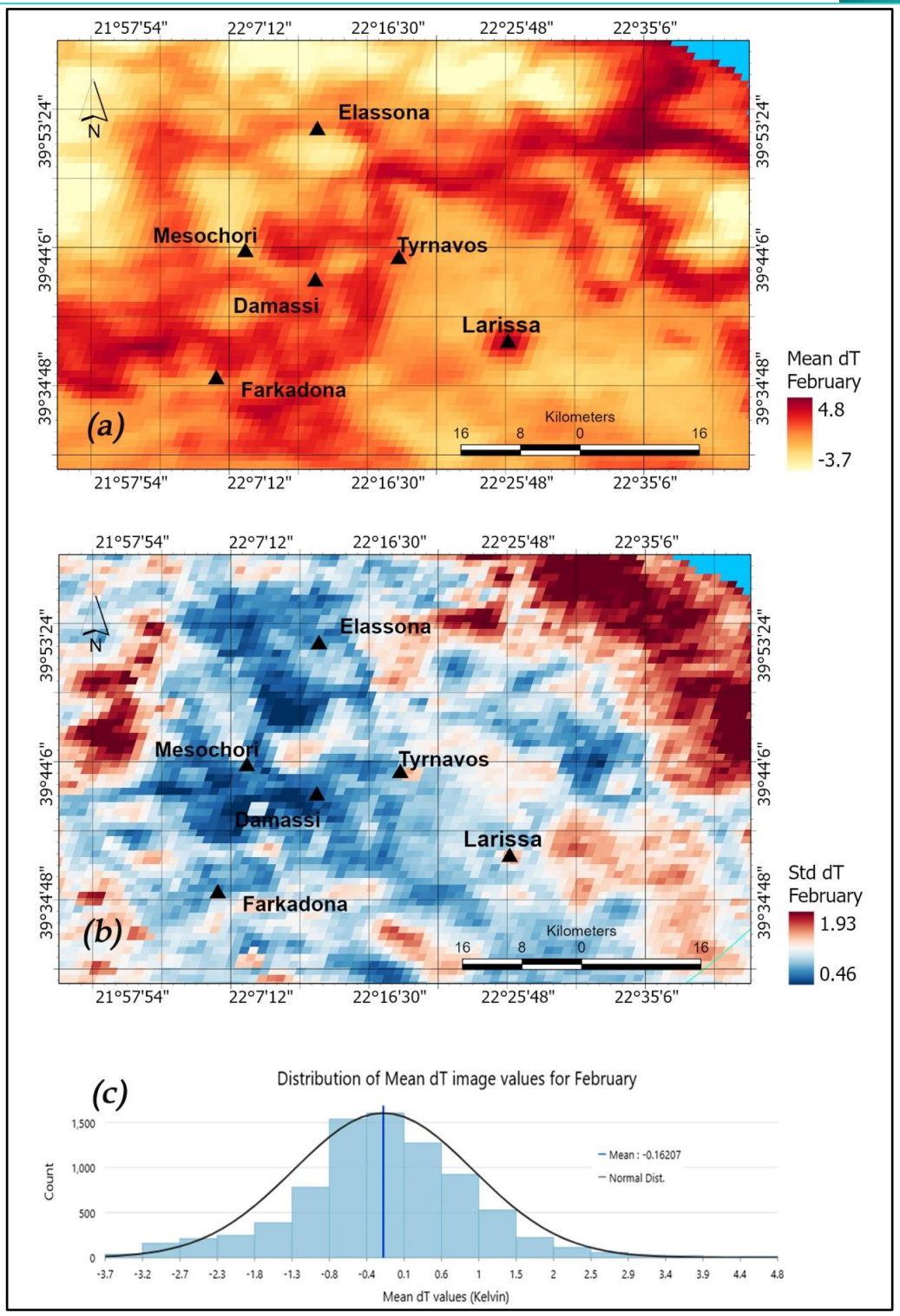

Fig. 2: Monthly Reference fields $\mu_{\Delta T}(x,y)$ and $\sigma_{\Delta T}(x,y)$ calculated for February using MODIS LST images acquired over the broader Larissa area from 2012 to 2021. The histogram showing the frequency distribution of the $\mu_{\Delta T}(x,y)$ (in Kelvin) is also given.

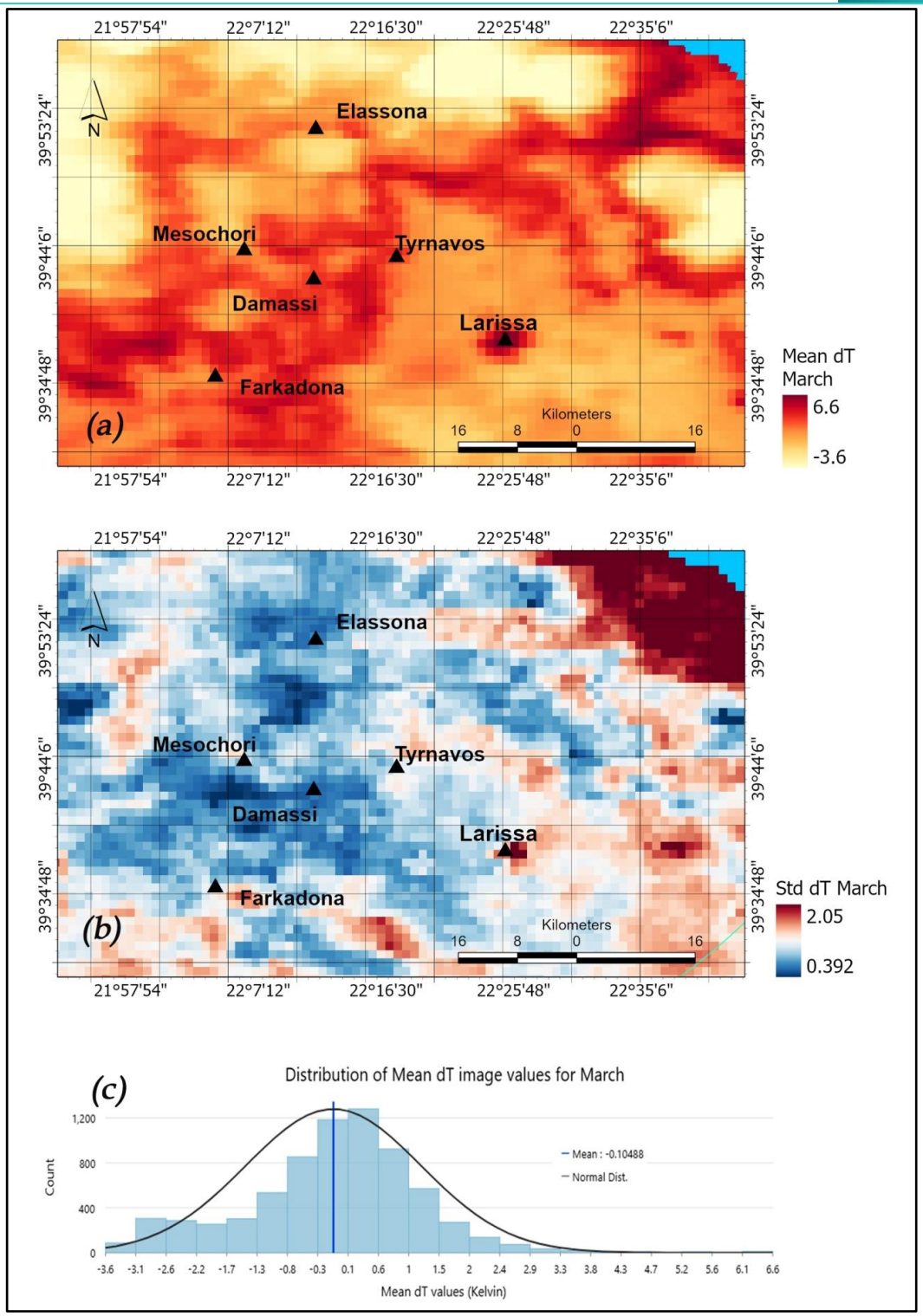

Fig. 3: Monthly Reference fields $\mu_{\Delta T}(x,y)$ and $\sigma_{\Delta T}(x,y)$ calculated for March using MODIS LST images acquired over the broader Larissa area from 2012 to 2021. The histogram showing the frequency distribution of the $\mu_{\Delta T}(x,y)$ (in Kelvin) is also given.

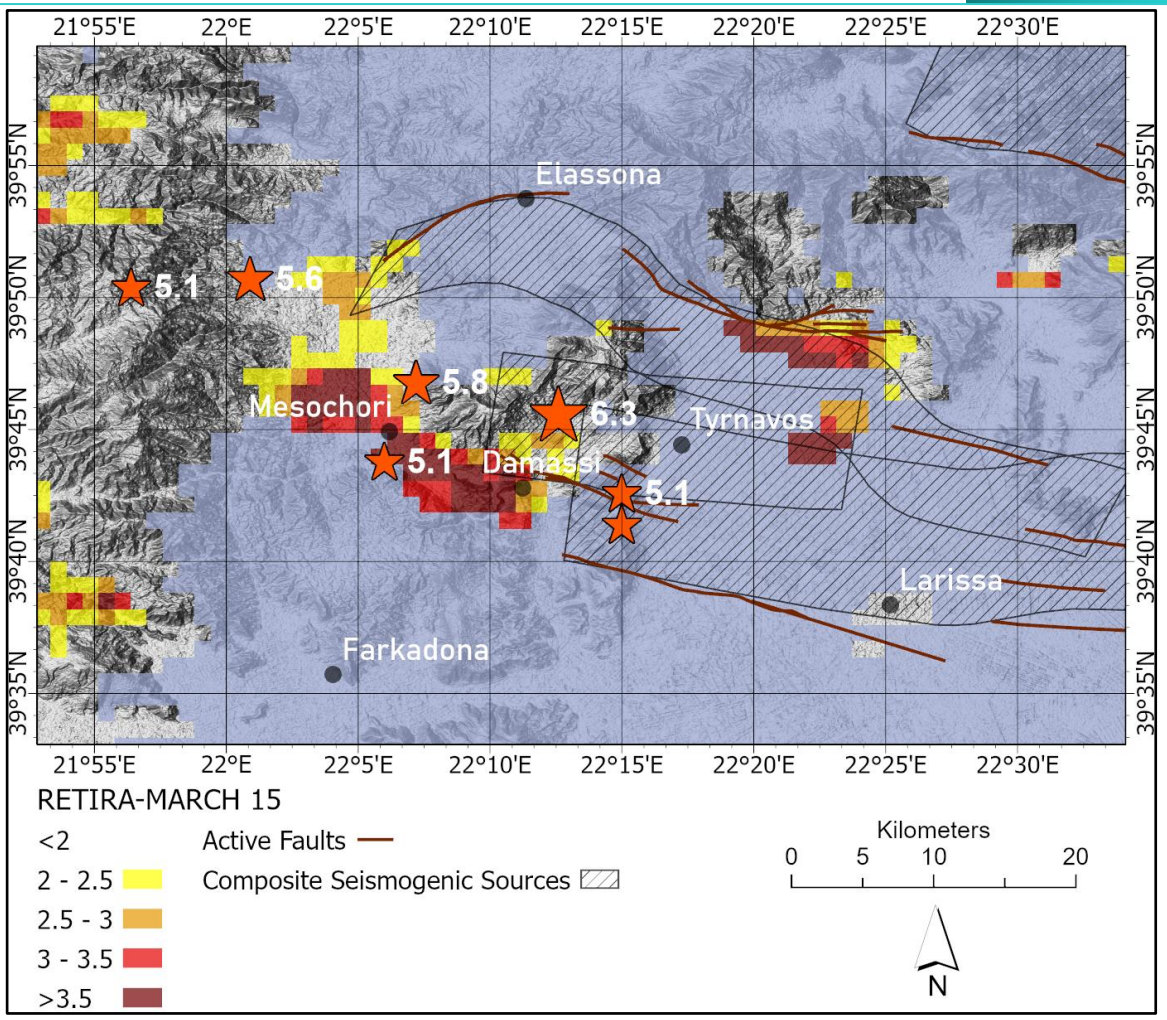

Fig. 4: Example of a false RETIRA thermal anomaly map. This pattern of artifacts is characterized from high RETIRA values located along the boundaries of cloudy pixels (violet areas) with the land pixels. Such images were excluded for further analysis.

4. RESULTS AND DISCUSSION

In this section, results achieved using the RETIRA index are presented and discussed. As we have already mention, the daily analysis revealed that 9 over 34 images included anomalous pixels with RETIRA values higher than 2.5. It is worth mentioning that 2 out of the 9 images were characterized as false thermal anomalies due to clouds. For instance, Fig. 4 shows a false thermal anomaly mapped on 15 March 2021 and excluded from further analysis since the anomalous pixels are induced due to cloud coverage. The 2 images were identified with on-screen interpretation and were immediately excluded. In this case we cannot talk about a false alarm. We consider a false alarm to exist when the index shows abnormal values that are not due or induced by a known cause and within a period of 15 days before them or 30 days after them there has been no earthquake occurrence with M> 4 in the research area (Eleftheriou et al., 2016a).

Unfortunately, due to the bad meteorological conditions we were not able to depict in detail the time persistence of thermal anomalies. This is the case of missing values and depends directly on the time of observations. In our case the sequence of the 7 thermal anomalies, 3 before the main earthquake, 1 on the day of the earthquake and another 3 after it, constitutes a successful application of the RETIRA index. Quite intense (Signal/Noise > 2.5) and rare, spatially extensive and time persistent, TIR signal transients were identified, appearing twenty-five, twenty and two days before the Thessaly main shock (pre-seismic anomalies: February 6th, February 11th March 1st), the day of the main earthquake (co-seismic anomaly) and one day, seven days and fourteen days after the main shock (post-seismic anomalies: March 4th, 10th and 17th) (Figs 5, 6 and 7). As shown in Figs. 5, 6 and 7, in some cases there are pixels with values up to 5 and this fact is an indication of the intensity of the anomalies (see dark brown pixels). Hence, we introduced the seven mapped thermal anomalies along with several geological elements, such as active faults and seismogenic sources in a Geographic Information System (GIS) (Figs 5, 6 and 7).

Regarding the preseismic thermal activity of the region of interest, on the 6th of February the thermal anomalies appear East of Elassona, near the village of Farkadona while there are few pixels in the western part of the area of interest (Fig 5). On February 11 (20 days before the main earthquake), the thermal anomalies are oriented ESE–WNW and are concentrated within the composite seismogenic zone located in the Tyrnavos basin. Near the village Damassi, almost at the point where the main earthquake occurred, they cross a second, NE-SW oriented zone defined by thermal anomalies (Fig 5). On March 1, the clouds allow us to see only scattered thermal anomalies. In many cases these anomalies are spatially limited by the existence of faults as in the case south of Farkadona (Fig. 5). On the day of the earthquake, the thermal anomalies appear in 3 areas: in the area between the epicenters of the main earthquake and the main aftershock that followed a day later, northeast of the village of Farkadona and in a N-W oriented zone east of the village of Mesochori (Fig.6). Finally, regarding the post-seismic thermal anomalies, on March 4 they are concentrated exclusively NE of Elassona (Fig. 7), on March 10 they present a spatial distribution similar to the distribution of February 11 and are controlled spatially by the ruptured zones as in the case north of Damassi village (Fig. 7). On March 17, the thermal anomalies occupy an extended area defined by the villages of Damassi, Farkadona Tyrnavos and reach very close to Larissa (Fig. 7).

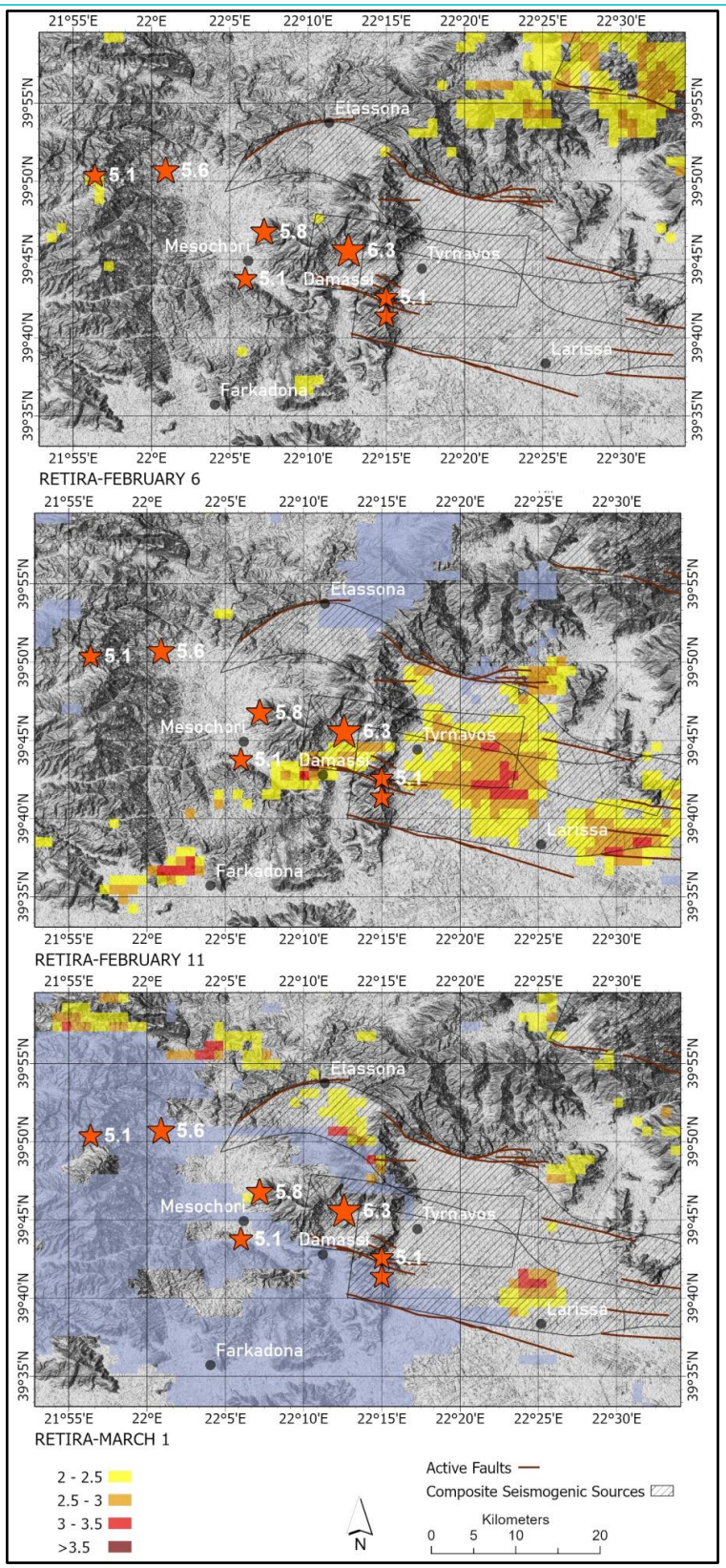

Fig. 5 Preseismic RETIRA thermal anomaly maps of the broader earthquake area combined with the active faults and seismogenic sources. Significant thermal anomalies were identified 25 (February 6th), 20 (February 11th) and 2 (March 1st) days before the main shock and are presented with different colors depending on their RETIRA value. The maps are draped over shaded relief. Cloud coverage is given with violet color.

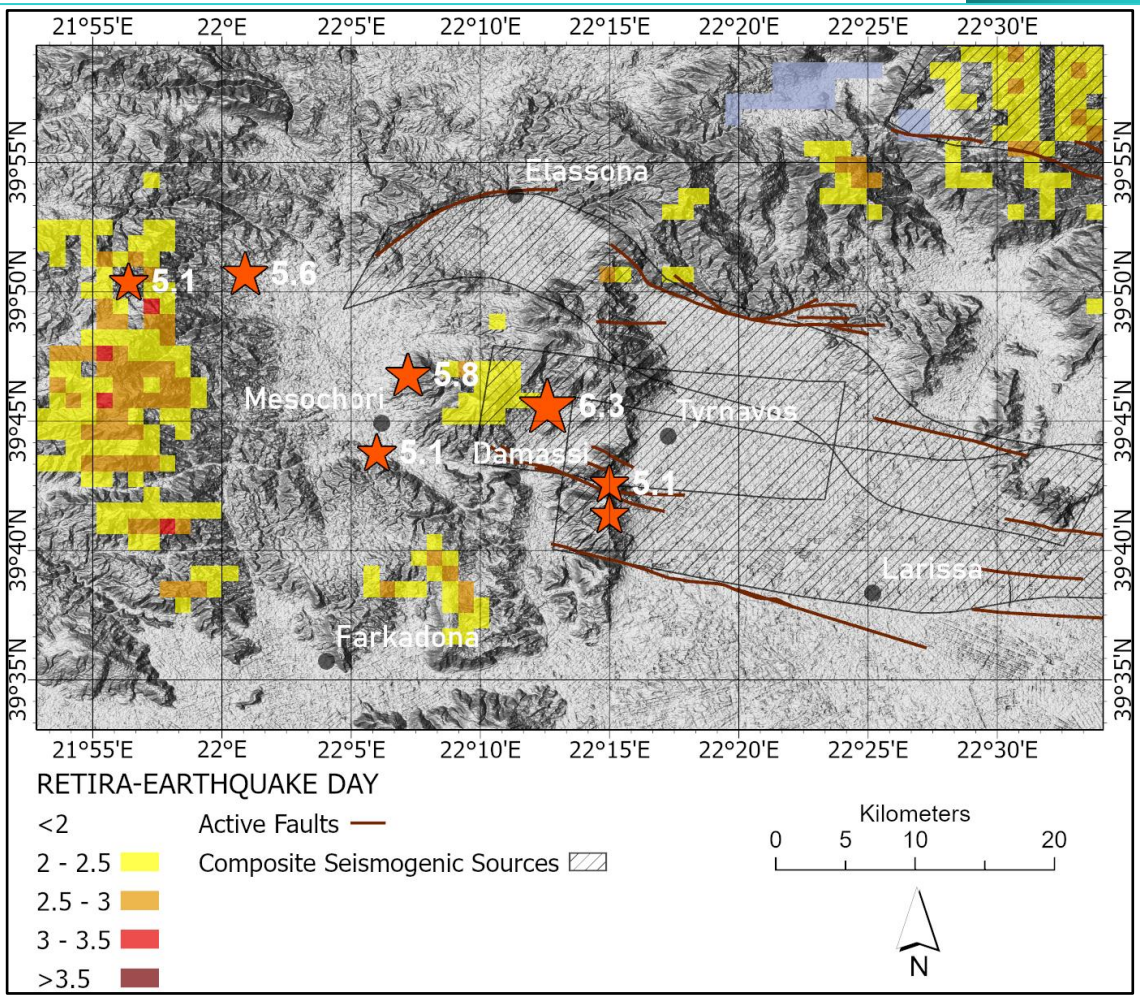

Fig. 6: Coseismic RETIRA thermal anomaly map of the broader earthquake area combined with the active faults and seismogenic sources. Significant thermal anomalies are presented with different colors depending on their RETIRA value. The map is draped over shaded relief. Cloud coverage is given with violet color. The MODIS scene has been acquired the night of March 3, 2021.

The total number of pixels characterized as thermally anomalous at least in one out of the seven RETIRA maps is 744. Moreover, the cumulative maps of Fig. 8 show the frequency of occurrence of thermal anomalies (i.e., the number of times over-threshold values are reached) during the 7 days represented by the RETIRA index maps for each pixel with RETIRA value greater than 2.5 (Fig. 8a) and for RETIRA value greater than 2.0 (Fig. 8b). In the aforementioned images, pixels characterized anomalous only once are not presented. In this way, we were able to define the areas in which the thermal anomalies are space-time persistent.

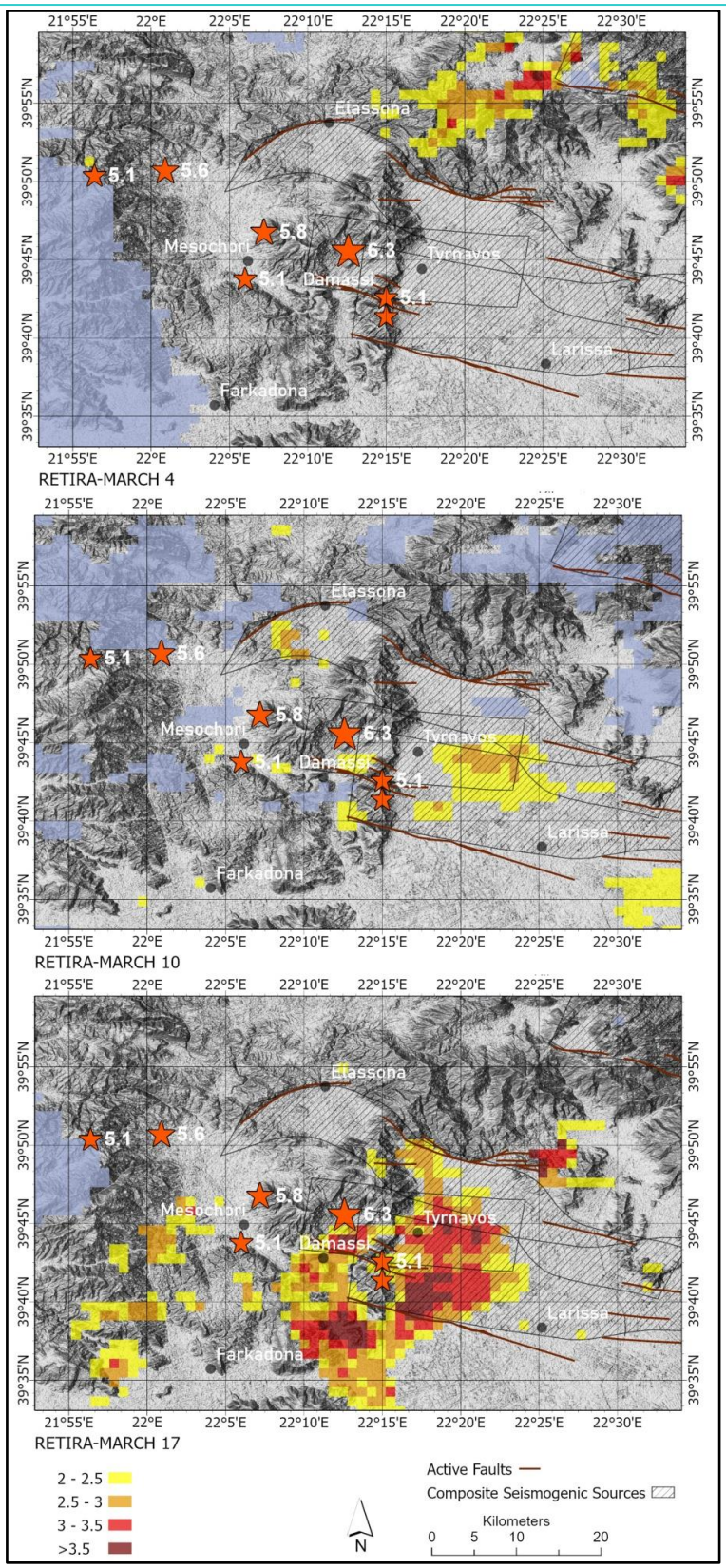

Fig. 7: Postseismic RETIRA thermal anomaly maps of the broader earthquake area combined with the active faults and seismogenic sources. Significant thermal anomalies were identified on March 4th, 10th and 17th and are presented with different colors depending on their RETIRA value. Cloud coverage is given with violet color. The maps are draped over shaded relief.

In the first case, 84 pixels with values 2 (75 pixels) and 3 (9 pixels) have been isolated; regarding the pixels equal to 2, two of them are located west of village Damassi, 5 in the area between Damassi and Tyrnavos, 54 in the area between Tyrnavos and Larissa, while the rest 14 are mainly located to the northeast of Tyrnavos basin. The nine pixels with value equal to 3 **(**i.e., these pixels were characterized as thermally anomalous the 3 out of the 7 days) are located east of Tyrnavos and they are surrounded from an extended area with value equal to 2 (Fig. 8a). The Fig. 8b shows the cumulative map when the RETIRA index threshold decreases to 2 instead of 2.5. As expected, the area covered by thermally anomalous pixels is more extended, as less intense anomalies are taken into account but the general spatial distribution pattern remains the same.

Preferential spatial distribution of anomalies over time seems to be concentrated inside the composite seismogenic sources and to be controlled by the existence of the active faults. In some cases, thermally anomalous pixels are located in the junction of two faults. A probable explanation could be the uplifting of the fluids and/or gasses through the tectonic faults due to changes of the sub-surface physicochemical processes. For instance, micro-fracturing can lead to permeability changes and gas diffusion, which supported by their high mobility (Conti et al., 2021; Martinelli, 2021). As stated by Pulinets and Ouzounov (2011), increase of stress can cause release of CO_2, CH_4, N_2O (greenhouse gases) that are trapped in the pores of rock, this can cause a local greenhouse effect). In addition, we note that the opening of microfractures has been suggested as a source of electrical precursors which some of the cases are related with the observations of gas emissions (see Vallianatos et al., 2004 and references therein).

Finally, preliminary spatial analysis of the number of times over-threshold values are reached, shows that the thermally anomalous pixels are hosted mainly by Quaternary deposits (Fig. 9), probably due to their high permeability. Taking into account all the pixels which showed thermally anomalous behavior at least in one out of the seven RETIRA maps (744 pixels in total)**,** the majority of them is detected in elevations lower than 350 m (Fig. 10a) and within a distance of 4 km from the faults (Fig. 10b).

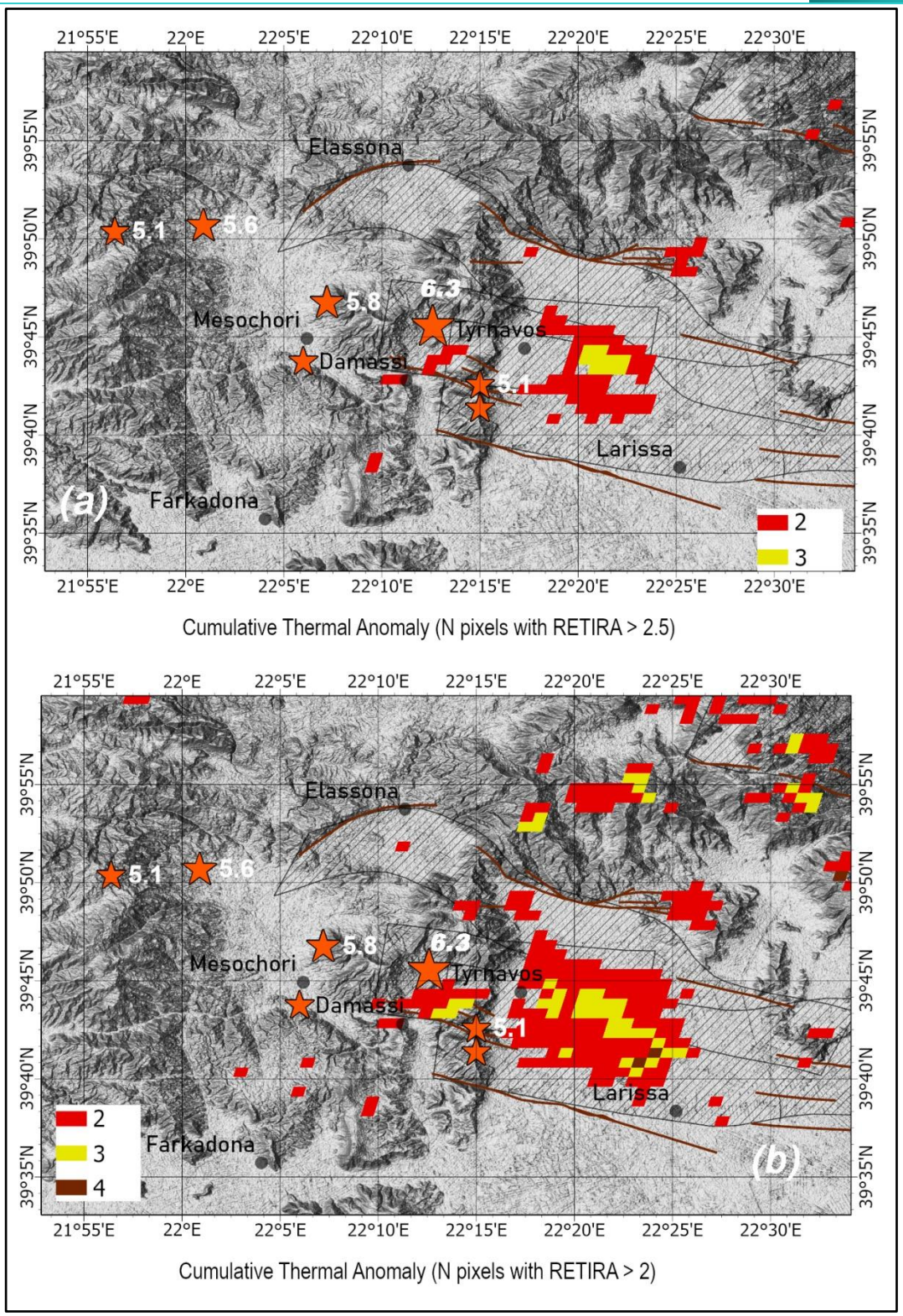

Fig. 8: Cumulative maps counting for each pixel the number of times over-threshold values (i.e., RETIRA index greater than 2.5 and 2.0) are reached for the seven days of thermal anomalies. These products cover a period of time from February 6 to March 17.

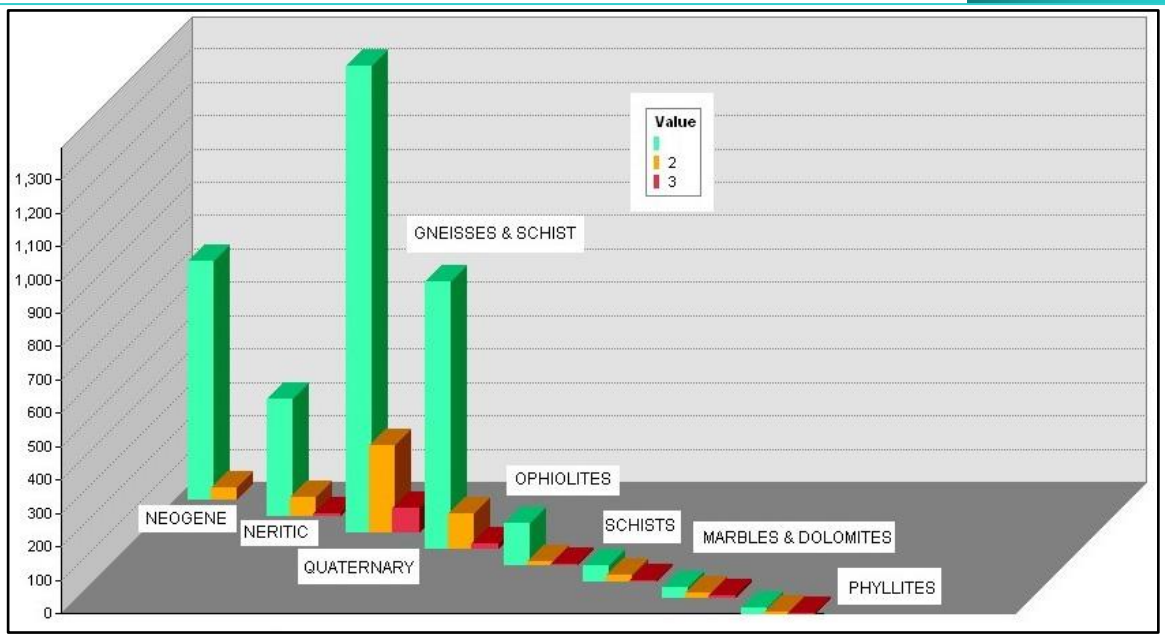

Fig. 9: The frequency distribution of cumulative thermal anomalies (based on Fig. 8b) within the different geological formations of the study area. With the green color is shown the total number of pixels in the geological formations.

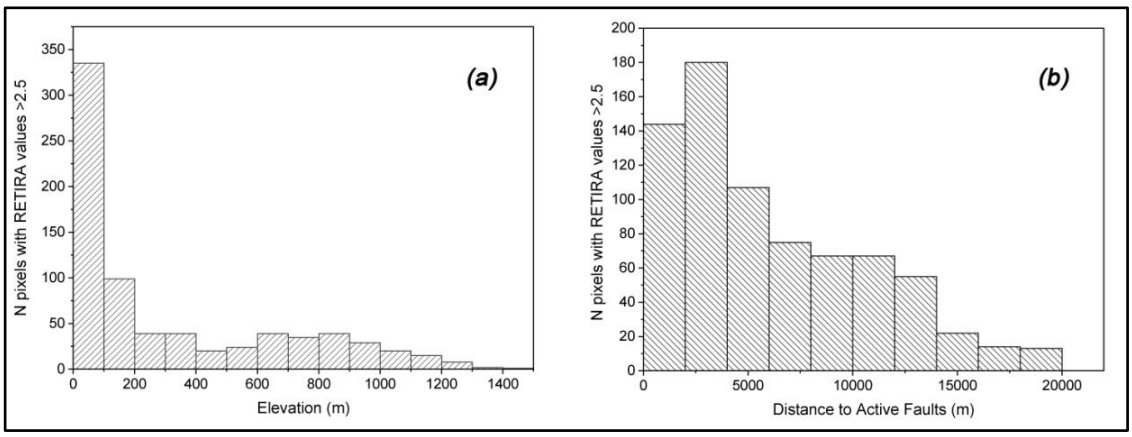

Fig. 10: The frequency distribution of all the thermally anomalous pixels (y-axis, 744 pixels in total) with respect to (a) the elevation and (b) the distance to active faults.

5. CONCLUSIONS

In the present work, MODIS (LST) data from a time-period of 10 years (2012-2021) were coupled with robust satellite technique and especially RETIRA index, with the aim to detect anomalous signal variations ascribable to Thessaly's earthquake sequence. We managed to detect preseismic, coseismic and post seismic thermal anomalies. The detected anomalies show a close spatial relation with the previously known seismogenic sources and the tectonic lineaments located in the area. Building up a system based on continuously updated observations, provided that they are adequately selected and

analyzed, may represent a hopeful research line to actually exploit accumulated knowledge of seismic hazard. In this direction, the RST technique and the long-term satellite thermal imagery processing combined with geological data can be proved a valuable tool.

6. ACKNOWLEDGMENTS

We acknowledge support of this study by the project "HELPOS - Hellenic Plate Observing System" (MIS 5002697) which is implemented under the Action "Reinforcement of the Research and Innovation Infrastructure", funded by the Operational Programme "Competitiveness, Entrepreneurship and Innovation" (NSRF 2014-2020) and co-financed by Greece and the European Union (European Regional Development Fund).

7. REFERENCES

Aguilar-Lome J., Espinoza-Villar R., J.C. Espinoza, J. Rojas-Acuña, B.L. Willems & W.M. Leyva-Molina, 2019. Elevation-dependent warming of land surface temperatures in the Andes assessed using MODIS LST time series (2000–2017). *Int J Appl Earth Obs.*, 77, pp 119-128 https://doi.org/10.1016/j.jag.2018.12.013

Aliano C., Corrado R., Filizzola C., Genzano N., Pergola N. & V. Tramutoli, 2008a. Robust TIR satellite techniques for monitoring earthquake active regions: limits, main achievements and perspectives. *Ann Geophys.*, 51, 303-317 https://doi.org/10.4401/ag-3050

Aliano C., Corrado R., Filizzola C., Pergola N. & Tramutoli V., 2008b. Robust satellite techniques (RST) for the thermal monitoring of earthquake prone areas: the case of Umbria-Marche October, 1997 seismic events. *Ann Geophys.*, 51, 451-459 https://doi.org/10.4401/ag-3025

Anderson M. & Kustas W., 2008. Thermal remote sensing of drought and evapotranspiration. *EOS T Am Geophys Un.*, 89 pp. 233-234 https://doi.org/10.1029/2008EO260001

Anderson M.C., Allen R.G., Morse A., Kustas W.P., 2012. Use of Landsat thermal imagery in monitoring evapotranspiration and managing water resources. *Remote Sens. Environ,* 122, pp 50-65 https://doi.org/10.1016/j.rse.2011.08.025

Athanasiadou, L., Psomiadis, E., & Stamatis, G. 2020. Thermal Remote Sensing for Water Outflows Detection and Determination of the Role of Lineaments in Underground Hydrodynamics of Evia Island, Central Greece. *Bulletin of the Geological Society of Greece, 56*(1), 100-132. https://doi.org/10.12681/bgsg.20948

Athanassiou A., 2002. Neogene and Quaternary mammal faunas of Thessaly. *Annales Géologiques des PaysHelléniques*, XXXIX (A), 279–293.

Brunsell N.A. & Gillies R.R., 2003. Determination of scaling characteristics of AVHRR data with wavelets: Application to SGP97. *Int. J. Remote Sens*., 24, pp 2945-2957 https://doi.org/10.1080/01431160210155983

Caputo R. and Pavlides S., 2013. The Greek Database of Seismogenic Sources (GreDaSS), version 2.0.0: A compilation of potential seismogenic sources (Mw > 5.5) in the Aegean Region. *doi: 10.15160/unife/gredass/0200*.

Caputo R., Bravard J.-P., Helly B., 1994. The Pliocene-Quaternary tecto-sedimentary evolution of the Larissa Plain (Eastern Thessaly, Greece). *Geodinamica Acta*, 7, pp. 57-85 https://doi.org/10.1080/09853111.1994.11105267

Caputo R., Pavlides S., 1993. Late Cainozoic geodynamic evolution of Thessaly and surroundings (central-northern Greece). *Tectonophysics*, 223, pp. 339-362 https://doi.org/10.1016/0040-1951(93)90144-9

Caputo R., Piscitelli S. , Oliveto A. , Rizzo E. , Lapenna V., 2003. The use of electrical resistivity tomography in active tectonics. Examples from the Tyrnavos Basin, Greece. *J. Geodyn*., 36 (1–2), pp. 19-35 10.1016/S0264-3707(03)00036-X

Caputo, R. 1990. Geological and structural study of the recent and active brittle deformation of the Neogene-Quaternary basins of Thessaly (Greece). In: *Scientific Annals, Vol. 12, Aristotle University of Thessaloniki, Thessaloniki.*

Christman Z., Rogan J., Eastman J.R. & Turner B.L., 2016. Distinguishing Land Change from Natural Variability and Uncertainty in Central Mexico with MODIS EVI, TRMM Precipitation, and MODIS LST Data. *Remote Sens*., 8, pp 478 https://doi.org/10.3390/rs8060478

Conti L., Picozza P. and Sotgiu A., 2021. A Critical Review of Ground Based Observations of Earthquake Precursors, Front. Earth Sci., 06 July 2021, https://doi.org/10.3389/feart.2021.676766

Eleftheriou A., Filizzola C., Genzano N., Lacava T., Lisi M., Paciello R., Pergola N., Vallianatos F. & Tramutoli V., 2016a. Long-term RST analysis of anomalous TIR sequences in relation with earthquakes occurred in Greece in the period 2004–2013. *Pure Appl. Geophys*., 173, pp 285-303 https://doi.org/10.1007/s00024-015-1116-8

Eleftheriou D., Kiaghidis K., Kalmintzis G., Kalea A., Bantasis C., Koumadoraki P., Spathara M.E., Tsolaki A., Tzampazidou M.I., Gemitzi A., 2016b. Determination of annual and seasonal daytime and nighttime trends of MODIS LST over Greece-climate change implications. *Sci. Total Environ*., 616, pp 937-947 doi: 10.1016/j.scitotenv.2017.10.226

Filizzola C., Pergola N., Pietrapertosa C. & Tramutoli V., 2004. Robust satellite techniques for seismically active areas monitoring: a sensitivity analysis on September 7, 1999 Athens's earthquake. *Phys. Chem. Earth*, PT A/B/C, 29, pp 517-527 DOI: 10.1016/j.pce.2003.11.019

Ganas, A., Lagios, E., Petropoulos, G. and Psiloglou, B., 2010. Thermal imaging of Nisyros volcano (Aegean Sea) using ASTER data: estimation of radiative heat flux, *International Journal of Remote Sensing*, 31: 15, 4033 — 4047 https://doi.org/10.1080/01431160903140837

Ganas, A., Oikonomou, I. & Tsimi, C., 2013. NOAfaults: a digital database for active faults in Greece, Bulletin of the Geological Society of Greece, 47: 2, 518 – 530 https://doi.org/10.12681/bgsg.11079

Ganas, A., Valkaniotis, S., Briole, P., Serpetsidaki, A., Kapetanidis, V., Karasante, I., Kassaras, I., Papathanassiou, G., Karamitros, I., Tsironi, V., Elias, P., Sarhosis, V., Karakonstantis, A., Konstantakopoulou, E., Papadimitriou, P., & Sokos, E., 2021. Domino-style earthquakes along blind normal faults in Northern Thessaly (Greece): kinematic evidence from field observations, seismology, SAR interferometry and GNSS. *Bulletin of the Geological Society of Greece*, 58, 37-86. https://doi.org/10.12681/bgsg.27102

Genzano N., Filizzola C., Lisi M., Pergola N., Tramutoli V., 2020. Toward the development of a multi parametric system for a short-term assessment of the seismic hazard in Italy. *Annals of Geophysics*, 63-5, PA550 https://doi.org/10.4401/ag-8227

Karnieli A., Agam N., Pinker R.T., Anderson M., Imhoff M.L., Gutman G.G., Panof N. & Goldberg A., 2010. Use of NDVI and land surface temperature for drought assessment: Merits and limitations. *J. Climate*, 23, pp 618-633. https://doi.org/10.1175/2009JCLI2900.1

Keramitsoglou I., Chris T., Kiranoudis C.T., Ceriola G., Weng Q., Rajasekar U., 2011. Identification and analysis of urban surface temperature patterns in Greater Athens, Greece, using MODIS imagery. *Remote Sens. Environ.*, 115, pp 3080-3090. https://doi.org/10.1016/j.rse.2011.06.014

Kustas W. & Anderson M., 2009. Advances in thermal infrared remote sensing for land surface modeling. *Agr. Forest Meteorol.*, 149, pp 2071-2081. https://doi.org/10.1016/j.agrformet.2009.05.016

Li Z.L., Tang B.H., Wu H., Ren H., Yan G., Wan Z. & Sobrino J.A., 2013. Satellite-derived land surface temperature: Current status and perspectives. *Remote Sens. Environ.*, 131, pp 14-37 https://doi.org/10.1016/j.rse.2012.12.008

Lillesand T. M., Kiefer R. W. & Chipman J. W.,1987. *Remote sensing and image interpretation.* John Wiley & Sons, New York.

Martinelli G., 2020. Previous, Current, and Future Trends in Research into Earthquake Precursors in Geofluids, *Geosciences*, 10, 189; https://doi.org/10.3390/geosciences10050189

Mavroulis, S., Mavrouli, M., Carydis, P., Agorastos, K., & Lekkas, E., 2021. The March 2021 Thessaly earthquakes and their impact through the prism of a multi-hazard approach in disaster management. *Bulletin of the Geological Society of Greece*, 58, 1-36. https://doi.org/10.12681/bgsg.26852

Pavlidou E., van der Meijde M., van der Werff H. and Hecker C., 2019, Time Series Analysis of Land Surface Temperatures in 20 Earthquake Cases Worldwide, *Remote Sensing*, 11, 61; doi:10.3390/rs11010061

Peleli, S., Kouli, M., Marchese, F., Lacava, T., Vallianatos, F., Tramutoli, V., 2021. Monitoring temporal variations in the geothermal activity of Miocene Lesvos volcanic field using remote sensing techniques and MODIS – LST imagery. *International Journal of Applied Earth Observation and Geoinformation*, 95, 102251. https://doi.org/10.1016/j.jag.2020.102251

Pulinets S. & Ouzounov D., 2011. Lithosphere–atmosphere–ionosphere coupling (LAIC) model–an unified concept for earthquake precursors validation *J. Asian Earth Sci.* 41 371–82. https://doi.org/10.1016/j.jseaes.2010.03.005

Scambos T. A., Campbell G. G., Pope A., Haran T., Muto A., Lazzara M., Reijmer C.H. and van den Broeke M.R., 2018. Ultralow surface temperatures in East Antarctica from satellite thermal infrared mapping: The coldest places on Earth *Geophys Res Lett.*, 45, pp 6124–6133 https://doi.org/10.1029/2018GL078133

Tramutoli V., 2007. Robust Satellite Techniques (RST) for Natural and Environmental Hazards Monitoring and Mitigation: Theory and Applications. *Int. Work. Anal. Multi-temporal Remote Sens. Images. IEEE*, pp 1–6 10.1109/MULTITEMP.2007.4293057

Tramutoli V., Di Bello G., Pergola N. & Piscitelli S., 2001. Robust satellite techniques for remote sensing of seismically active areas. *Ann di Geofis*., 44, pp 295–312 https://doi.org/10.4401/ag-3596

Tramutoli V., Cuomo V., Filizzola C., Pergola N. & Pietrapertosa C., 2005. Assessing the potential of thermal infrared satellite surveys for monitoring seismically active areas: The case of Kocaeli (Izmit) earthquake, August 17, 1999. *Remote Sens Environ*., 96, pp 409-426 10.1016/j.rse.2005.04.006

Vallianatos F., Triantis D., Tzanis A., Anastasiadis C., Stavrakas I., 2004. Electric earthquake precursors: from laboratory results to field observations, *Physics & Chemistry of the Earth*, 29, 339-351. DOI: 10.1016/j.pce.2003.12.003

Vassilopoulou S., Sakkas V., Wegmuller U., Capes R. 2013. Long Term and Seasonal Ground Deformation Monitoring of Larissa Plain (Central Greece) by Persistent Scattering Interferometry, *Cent. Eur. J. Geosci.*, 5(1), pp 61-76. https://doi.org/10.2478/s13533-012-0115-x

Vollmer M., Möllmann K.P., 2017. Infrared thermal imaging: fundamentals, research and applications, *John Wiley & Sons, 2nd Edition*. ISBN: 978-3-527-41351-5

Wan Z., 2013. MODIS Land Surface Temperature products user's guide. *https://icess.eri.ucsb.edu/modis/LstUsrGuide/usrguide.html*

Williamson S. N., Hik D. S., Gamon J. A., Kavanaugh J. L. and Koh S., 2013. Evaluating cloud contamination in clear-sky MODIS Terra daytime land surface temperatures using ground-based meteorology station observations, *J. Clim.*, 26(5), 1551–1560. https://doi.org/10.1175/JCLI-D-12-00250.1

Zhang Y., Jiang Z., Huang H., FanG Y., Mu X. and Cheng X., 2014. Thermal Anomalies Detection before 2013 Songyuan earthquake using MODIS LST data, *IGARSS 2014, doi: 10.1109/IGARSS.2014.6947110*